IET Microwaves, Antennas & Propagation

Research Article

IET Journals
The Institution of Engineering and Technology

Modelling cascaded cylindrical metasurfaces using sheet impedances and a transmission matrix formulation

ISSN 1751-8725
Received on 14th June 2017
Revised 15th December 2017
Accepted on 26th December 2017
E-First on 22nd March 2018
doi: 10.1049/iet-map.2017.0465
www.ietdl.org

Zvonimir Sipus[1] ✉, *Marko Bosiljevac*[1], *Anthony Grbic*[2]

[1]*Faculty of Electrical Engineering and Computing, University of Zagreb, Unska 3, Zagreb, Croatia*
[2]*Department of Electrical Engineering and Computer Science, University of Michigan, Ann Arbor, USA*
✉ *E-mail: zvonimir.sipus@fer.hr*

Abstract: Metasurfaces that manipulate electromagnetic waves have gained significant attention in recent years. The focus has primarily been on planar devices, while many applications require curved surfaces. In this study, the authors propose an analysis approach for cylindrical cascaded (multilayer) metasurfaces. The approach combines the concept of sheet impedance in the spectral domain with a new transmission matrix formulation that is applicable to stratified, canonical curved geometries. Approximate formulas for the sheet impedance of common planar, metallic patterns are also adapted to curved geometries. The reported analysis approach allows one to determine the optimal spectral-domain, azimuthal dependence of a sheet impedance, as well as the best geometrical elements to obtain the required azimuthal variation. The results are verified through several cylindrical metsurface examples.

1 Introduction

Electromagnetic (EM) metamaterial structures and surfaces have attracted strong interest over the past several years. While this interest has resulted in very interesting designs (e.g. EM cloaks and superlenses), it has also initiated research in other directions. In particular, new possibilities for manipulating the direction and polarisation properties of transmitted EM waves have been explored. Traditionally, resonant elements were used in the design of periodic frequency selective surfaces [1]. The more recent use of sub-wavelength elements as building blocks for metasurfaces has enabled a wider range of functionality such as focusing, beam tilting, polarisation manipulation, and increased bandwidth and angular performance (see e.g. [2–5]).

Studies to date have predominantly considered planar surfaces that can be realised using conventional planar fabrication techniques. For such surfaces, efficient design approaches based on surface impedance boundary conditions (both penetrable [3, 4, 6–11] and opaque surface impedance formulations [4, 12, 13]) have been developed. However, either for mechanical/aerodynamic, or EM reasons, some metasurface designs require curvature. In general, introducing curvature to metasurface design is a challenging task, since one needs to deal with finite dimensions and a more complex periodicity. Several other difficulties arise when translating analysis and design approaches from planar to curved structures. For example, the projection of a periodic grid onto curved surfaces becomes an issue, and incident plane waves are scattered as a spectrum of reflected waves, as opposed to a single plane wave in the planar case. Cylindrical metasurfaces, fabricated from flexible printed circuit boards, have been considered in the past as attractive class of curved metasurface structures. They were used for reshaping radiation patterns [14, 15], mantle cloak realisations [16, 17], the reduction of antenna blockage [18], and scattering manipulation and camouflage [19].

The focus of this paper is to introduce an analysis approach applicable to canonical curved metasurfaces; a detailed formulation is presented for cylindrical cascaded metasurfaces. The proposed analysis combines the concept of sheet impedances in the spectral domain with an ABCD transmission matrix formula to allow the analysis of multilayer structures. In other words, the ABCD matrix formulation for the analysis of cascaded circuit networks as well as planar, stratified EM structures is extended to cylindrical geometries. The influence of the higher order azimuthal modes is discussed in detail. To date, only the dominant zero-order cylindrical mode was considered to obtain a required metasurface reactance (see e.g. [16–19]). It will be shown that a metasurface's response to higher order modes (its response to the waves with azimuthal propagation constants different from zero) helps in selecting optimal metasurface elements/textures for a given application. Furthermore, the analytical formulas for the sheet impedance of commonly used planar, metallic patterns are modified to account for curvature.

The first part of the paper describes both the analysis of single-layer, cylindrical metasurfaces and an ABCD transmission matrix approach for cascaded, concentric structures. The proposed approach can be applied to cylindrical structures with various different layers (metallic or dielectric). This is exploited in the results section by first studying the accuracy of different methods for determining sheet impedances, followed by the investigation of situations where the dependence of sheet impedances on azimuthal modes has to be taken into account. Finally, two-sheet metasurface example is used to evaluate the number of cylindrical modes that are needed to accurately model the cascaded structures.

2 Theory

2.1 Analysis of single-layer cylindrical metasurface

The analysis will be performed in the spectral domain. That is, the EM fields are Fourier transformed along the two dimensions in which the structure is invariant. In the considered cylindrical case, we decompose the EM field into cylindrical waves (e.g. representation of the E-field)

$$\boldsymbol{E}(\rho,\phi,z)=\sum_{m=-\infty}^{\infty}\int_{-\infty}^{\infty}\tilde{\boldsymbol{E}}(\rho,m,k_z)\,\mathrm{e}^{-\mathrm{j}m\phi}\,\mathrm{e}^{-\mathrm{j}k_z z}\,\mathrm{d}k_z \tag{1}$$

For the considered cylindrical structure of circular cross-section, one can represent the field distribution in the nth layer in the following way:

$$\tilde{E}_z(\rho,m,k_z)=C_{1m}H_m^{(1)}(k_{\rho n}\rho)+C_{2m}H_m^{(2)}(k_{\rho n}\rho), \tag{2a}$$

$$\tilde{H}_z(\rho,m,k_z)=C_{3m}H_m^{(1)}(k_{\rho n}\rho)+C_{4m}H_m^{(2)}(k_{\rho n}\rho)\,. \tag{2b}$$

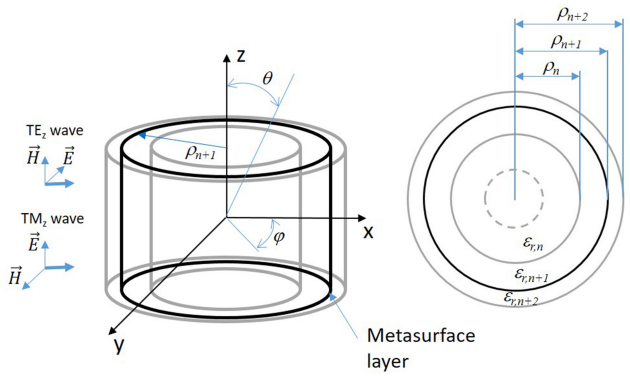

Fig. 1 *Geometry of curved metasurface structure*

Here $H_m^{(1)}$ and $H_m^{(2)}$ are the Hankel functions of the first and second kinds (they represent inward and outward travelling cylindrical waves), and C_m is the wave amplitude that needs to be determined. The other field components are determined using the following expressions:

$$\tilde{E}_\phi(\rho,m,k_z) = -\frac{mk_z}{k_{\rho n}^2\rho}\tilde{E}_z(\rho,m,k_z) + \frac{j\eta_n k_n}{k_{\rho n}^2}\frac{\partial}{\partial\rho}\tilde{H}_z(\rho,m,k_z) \quad (3a)$$

$$\tilde{H}_\phi(\rho,m,k_z) = -\frac{mk_z}{k_{\rho n}^2\rho}\tilde{H}_z(\rho,m,k_z) - \frac{jk_n}{\eta_n k_{\rho n}^2}\frac{\partial}{\partial\rho}\tilde{E}_z(\rho,m,k_z) \quad (3b)$$

The radial component of the propagation constant is defined as $k_{\rho n}^2 = k_n^2 - k_z^2$, and k_n and η_n are wave number and wave impedance of the considered layer.

For each spectral component, the metasurface layer is modelled using a penetrable sheet impedance boundary condition (an example of geometry is shown in Fig. 1)

$$\hat{n}\times\tilde{\boldsymbol{E}} = \hat{n}\times\left[\bar{\bar{Z}}\cdot\tilde{\boldsymbol{J}}_{av}\right] = \hat{n}\times\left[\bar{\bar{Z}}\cdot\left(\hat{n}\times\left(\tilde{\boldsymbol{H}}^+ - \tilde{\boldsymbol{H}}^-\right)\right)\right] \quad (4)$$

Here, $\tilde{\boldsymbol{E}}$ denotes one spectral component of the averaged electric field at a metasurface layer, $\tilde{\boldsymbol{H}}^+$ and $\tilde{\boldsymbol{H}}^-$ are the spectral components of the magnetic field at the outer and inner metasurface boundaries, $\tilde{\boldsymbol{J}}_{\text{av}} = \hat{n}\times(\tilde{\boldsymbol{H}}^+ - \tilde{\boldsymbol{H}}^-)$ represents the averaged surface current in the spectral domain, $\bar{\bar{Z}}$ is the sheet impedance tensor, and $\hat{n}$ is the outward pointing unit vector, normal to the metasurface layer ($\hat{n} = \hat{\rho}$). Note that the metasurfaces (see Fig. 1) introduce a discontinuity in the tangential magnetic field only. In other words, the metasurface only has an electric response, and can be modelled with induced surface electric currents. The generalisation to magnetic surface currents (loop or slotted metasurface elements) is straightforward.

The surface impedance tensor $\bar{\bar{Z}}$ is not a constant tensor but rather depends on the properties of the impinging EM wave. That is, the non-local (spatially dispersive) properties of the metasurface are taken into account. For instance, in the planar case, the non-local properties can be characterised by varying the incidence angle of the incoming plane wave. Therefore, for each spectral field component, we define the impedance tensor $\bar{\bar{Z}} = \bar{\bar{Z}}(m,k_z)$ that can be expressed as

$$\bar{\bar{Z}}(m,k_z) = \begin{bmatrix} Z_{\phi\phi}(m,k_z) & Z_{\phi z}(m,k_z) \\ Z_{z\phi}(m,k_z) & Z_{zz}(m,k_z) \end{bmatrix}. \quad (5)$$

Here, the subscripts denote the corresponding components of the electric field and surface current, respectively. Note that the spectral variable m corresponds to the transverse component of the wave number, $k_t = m/\rho_n$ where ρ_n is the radius of the considered metasurface layer. Given that azimuthal modes with $m \le k\rho_n$ are propagating, they need to be taken into account when calculating the scattered field. Since the sheet impedance depends on the azimuthal wave number, this dependency should also be taken into account in the calculation, as will be shown in the next section.

As (4) indicates, sheet impedances can be calculated from the calculated transverse components of the EM field on either side of the sheet. This can be done using a solver based on the moment method (MoM) [20] or other numerical methods. Often the cylindrical sheet impedance is approximated with the sheet impedance of an equivalent planar sheet. Alternatively, analytical sheet impedance formulas can be used that are available for commonly used planar patterns [21, 22]. In general, these two approximate approaches (note that both are planar approximations) do not account for the sheet impedance's dependence on the spectral variable m. However, the analytical sheet impedance formulas depend on the angle of incidence θ through the spectral variable $k_z = k_0\cos\theta$. Therefore, the azimuthal dependence of the sheet impedance can also be included by defining a tangential wavenumber that is azimuthal $k_\phi = m/\rho$. The accuracy of these two simplified methods for determining $\bar{\bar{Z}}$ will be discussed in the next section.

2.2 Analysis of cascaded cylindrical metasurface structures

In order to calculate the response of the cylindrical metasurface, consisting of a cascade of multiple layers, we will use a cylindrical ABCD transmission matrix approach [23]. This approach is a simple, yet powerful, tool that allows the analysis of multilayer, periodic canonical metasurfaces. One simply needs to analyse each layer separately (find the impedance tensor $\bar{\bar{Z}}$ of each cylindrical sheet and dielectric layer), and then multiply the ABCD matrices of the individual layers to obtain the overall ABCD matrix of the cascaded layers (the metasurface structure). This approach can also simplify the design/optimisation of these cascaded metasurfaces, since it becomes possible to separate the original complex problem into several simpler sub-problems.

Let us consider the case where one wishes to calculate the field scattered from an N-layer cylindrical metasurface. The spectral-domain ABCD matrix of a constitutive sheet of the metasurface is given by the following expression:

$$\begin{bmatrix} \tilde{E}_z \\ \tilde{H}_\phi^+ \\ \tilde{E}_\phi \\ \tilde{H}_z^+ \end{bmatrix} = \begin{bmatrix} 1 & 0 & 0 & 0 \\ Y_{zz} & 1 & Y_{z\phi} & 0 \\ 0 & 0 & 1 & 0 \\ -Y_{\phi z} & 0 & -Y_{\phi\phi} & 1 \end{bmatrix} \cdot \begin{bmatrix} \tilde{E}_z \\ \tilde{H}_\phi^- \\ \tilde{E}_\phi \\ \tilde{H}_z^- \end{bmatrix} \quad (6)$$

where $\bar{\bar{Y}} = \bar{\bar{Z}}^{-1}$. Both transverse electric (TE$_z$) and transverse magnetic (TM$_z$) waves along the z-axis are considered which leads to a 4×4 ABCD matrix [3]. It should be noted that all entries of the ABCD matrix are dependent on both azimuthal mode number m and wavenumber k_z.

The total fields in each dielectric layer can be written in terms of outward and inward travelling cylindrical waves (Hankel functions of the first and second kind, see (2) and (3)) as follows:

$$\begin{bmatrix} \tilde{E}_z(\rho) \\ \tilde{H}_\phi(\rho) \\ \tilde{E}_\phi(\rho) \\ \tilde{H}_z(\rho) \end{bmatrix} = M(\rho)\cdot\begin{bmatrix} \alpha^- \\ \alpha^+ \\ \beta^- \\ \beta^+ \end{bmatrix} \quad (7a)$$

(see (7b)) . Here, α and β are the amplitudes of the propagating, cylindrical TM and TE waves in the considered dielectric layer (i.e. the E_z and H_z components without the radial dependence), respectively. The superscripts + and − denote outward and inward cylindrical waves. The ABCD matrix can be solved by relating the field expressions at the two boundaries (inner with coordinate ρ_{n-1} and outer with coordinate ρ_n) of the cylindrical transmission line

$$M(\rho)=\begin{bmatrix} H_m^{(1)}(k_{\rho n}\rho) & H_m^{(2)}(k_{\rho n}\rho) & 0 & 0 \\ -\frac{jk_n}{\eta_n k_{\rho n}}H_m^{'(1)}(k_{\rho n}\rho) & -\frac{jk_n}{\eta_n k_{\rho n}}H_m^{'(2)}(k_{\rho n}\rho) & -\frac{mk_z}{k_{\rho n}^2\rho}H_m^{(1)}(k_{\rho n}\rho) & -\frac{mk_z}{k_{\rho n}^2\rho}H_m^{(2)}(k_{\rho n}\rho) \\ -\frac{mk_z}{k_{\rho n}^2\rho}H_m^{(1)}(k_{\rho n}\rho) & -\frac{mk_z}{k_{\rho n}^2\rho}H_m^{(2)}(k_{\rho n}\rho) & \frac{j\eta_n k_n}{k_{\rho n}}H_m^{'(1)}(k_{\rho n}\rho) & \frac{j\eta_n k_n}{k_{\rho n}}H_m^{'(2)}(k_{\rho n}\rho) \\ 0 & 0 & H_m^{(1)}(k_{\rho n}\rho) & H_m^{(2)}(k_{\rho n}\rho) \end{bmatrix} \tag{7b}$$

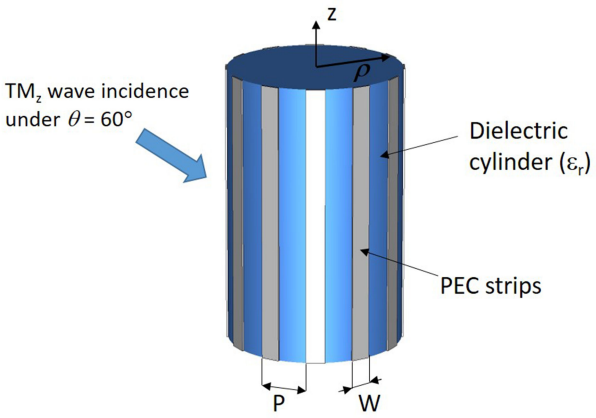

Fig. 2 *Dielectric cylinder with periodic vertical PEC strips*

$$\begin{bmatrix} \tilde{E}_z(\rho_n) \\ \tilde{H}_\phi(\rho_n) \\ \tilde{E}_\phi(\rho_n) \\ \tilde{H}_z(\rho_n) \end{bmatrix} = M(\rho_{n+1})\cdot M^{-1}(\rho_n)\cdot \begin{bmatrix} \tilde{E}_z(\rho_{n-1}) \\ \tilde{H}_\phi(\rho_{n-1}) \\ \tilde{E}_\phi(\rho_{n-1}) \\ \tilde{H}_z(\rho_{n-1}) \end{bmatrix} \tag{8}$$

It should be noted that the resulting ABCD matrix is block-diagonal for $k_z=0$ or for $m=0$. In other words, under normal incidence and for the fundamental ϕ-invariant mode, the TE$_z$ and TM$_z$ waves are uncoupled.

The ABCD matrix of the multilayer cylindrical metasurface structure is obtained by simply multiplying the ABCD matrices of the cascaded cylindrical transmission lines (dielectric layers) and the sheets. From it, the scattered field can be easily determined. One simply needs to solve the following matrix equation:

$$\begin{bmatrix} \tilde{E}_z^{\text{inc}}(\rho_N,m,k_z)+\tilde{E}_z^{\text{scat}}(\rho_N,m,k_z) \\ \tilde{H}_\phi^{\text{inc}}(\rho_N,m,k_z)+\tilde{H}_\phi^{\text{scat}}(\rho_N,m,k_z) \\ \tilde{E}_\phi^{\text{inc}}(\rho_N,m,k_z)+\tilde{E}_\phi^{\text{scat}}(\rho_N,m,k_z) \\ \tilde{H}_z^{\text{inc}}(\rho_N,m,k_z)+\tilde{H}_z^{\text{scat}}(\rho_N,m,k_z) \end{bmatrix} = \left\{\prod_i \begin{bmatrix} A & B \\ C & D \end{bmatrix}_i\right\}\cdot \begin{bmatrix} \tilde{E}_z(\rho_1,m,k_z) \\ \tilde{H}_\phi(\rho_1,m,k_z) \\ \tilde{E}_\phi(\rho_1,m,k_z) \\ \tilde{H}_z(\rho_1,m,k_z) \end{bmatrix}. \tag{9}$$

Here, the ABCD matrices of the metasurface layers and the cylindrical transmission lines are symbolically written; ρ_1 and ρ_N are the inner and outer boundaries of the entire structure. Matrix (9) represents a system of four equations with four unknowns: the amplitudes of $\tilde{E}_z$ and $\tilde{H}_z$ components at the inner and outer boundaries of the structure. The amplitudes of the ϕ-components are calculated using (3). From these EM field quantities, the scattered field can be found. For the EM field in the innermost layer the standing wave representation (i.e. the Bessel function representation) is applied in (2), thus we have only two unknown coefficients related to that layer. Therefore, the four unknowns in the linear system (9) are the amplitudes of the z-components of the scattered field and of the EM field in the innermost region.

In all the considered examples, the metasurface structures were excited with an incident plane wave

$$E_z^{\text{inc}} = E_0\sin\theta^{\text{inc}}\cos\alpha^{\text{inc}} \cdot \sum_{m=-\infty}^{\infty}(-j)^m J_m(k_0\rho\sin\theta^{\text{inc}})\mathrm{e}^{-\mathrm{j}m\phi}\mathrm{e}^{\mathrm{j}zk_0\cos\theta^{\text{inc}}} \tag{10a}$$

$$H_z^{\text{inc}} = \frac{E_0}{\eta_0}\sin\theta^{\text{inc}}\sin\alpha^{\text{inc}} \cdot \sum_{m=-\infty}^{\infty}(-j)^m J_m(k_0\rho\sin\theta^{\text{inc}})\mathrm{e}^{-\mathrm{j}m\phi}\mathrm{e}^{\mathrm{j}zk_0\cos\theta^{\text{inc}}} \tag{10b}$$

For $\alpha^{\text{inc}}=0°$ the excitation is a TM$_z$ plane wave and for $\alpha^{\text{inc}}=90°$ it is a TE$_z$ plane wave. Other types of excitations, like a line source, can be implemented in a straightforward manner (see e.g. [17]).

Note that the ABCD matrix approach can also be applied to cylindrical structures with only one metasurface layer, and the first set of results will consider such structures.

3 Results

3.1 Exact surface impedance versus approximations

The first set of results compares how different ways of calculating metasurface reactance affect the overall results. We start with case 1 where we calculated the field scattered by a dielectric cylinder covered with vertical strips under TM$_z$ incidence, as shown in Fig. 2. In this case, the metasurface acts as an inductive reactance.

The dielectric cylinder considered is made of Teflon with $\varepsilon_r=2.1$, $\tan\delta=0.00015$, and has a radius $\rho=12.7$ mm. The strip width is $W=3$ mm and the period of the strips is $P_\phi=9.97$ mm ($0.33\lambda_0$ at 10 GHz). The incident wave is TM$_z$ polarised with incident angle $\theta=60°$. In the past, such cylinders were manufactured and their scattering properties were measured at Chalmers University of Technology [20].

First, we tested the proposed analysis method for the case where the sheet impedance tensor $\bar{\bar{Z}}$ was calculated using a MoM code for cylindrical periodic structures [20]. As shown in Fig. 3, there is an excellent agreement between the calculated results obtained using the proposed method and the exact MoM code for cylindrical structures. There is also good agreement with the measurements of the experimental prototype, even with its fabrication tolerances.

Further, it is valuable to compare how different approximations for the sheet impedance tensor affect the results obtained using the proposed analysis approach. Two separate approximations were considered, and compared to the results obtained for the sheet impedance tensor calculated using the cylindrical MoM code. First, a MoM code for planar (flat) periodic structures was used to extract the impedance tensor at $\theta=60°$ incidence. Next, the following approximate expression for planar strips [21] was used for a TM$_z$ incident wave:

$$Z_{zz}^{\text{approx}}(k_z) = j\frac{k_0\eta_0}{2\pi}P_\phi\log\left(\csc\left(\frac{\pi W}{2P_\phi}\right)\right)\left(1-\frac{k_z^2}{k_{\text{eff}}^2}\right) \tag{11}$$

$$Z_{\phi\phi}^{\text{approx}}(k_z) = -j\frac{\pi\eta_0}{P_\phi k_0(1+\varepsilon_r)}\left[\log\left(\csc\left(\frac{\pi W}{2P_\phi}\right)\right)\left(1-\frac{k_z^2}{k_{\text{eff}}^2}\right)\right]^{-1} \tag{12}$$

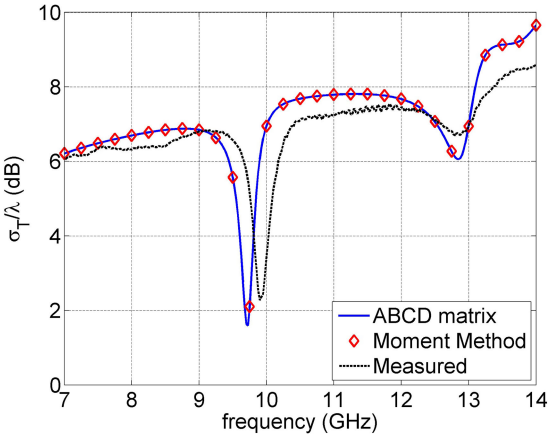

Fig. 3 *Total scattering width of a dielectric cylinder loaded with periodic axial strips*

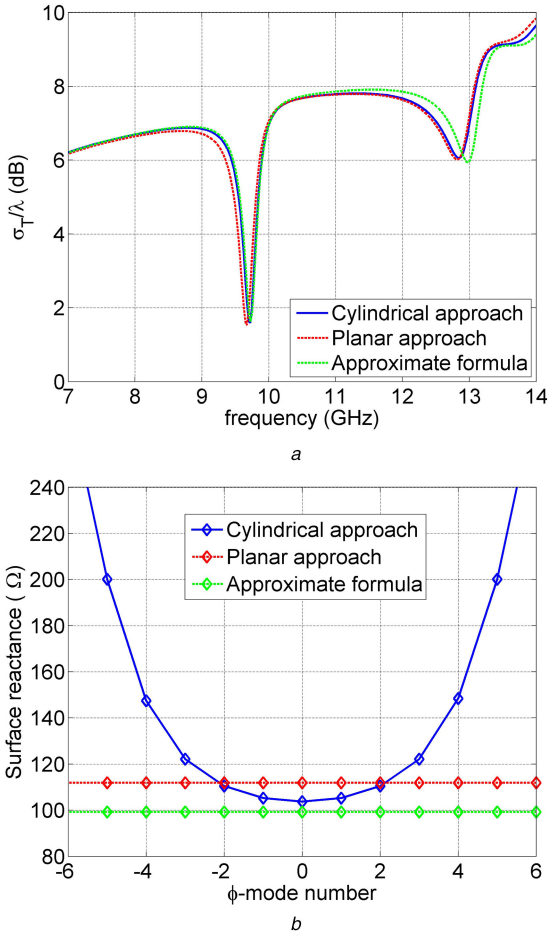

Fig. 4 *Comparison of calculated total scattering width of a dielectric cylinder loaded with periodic axial strips. The metasurface impedance is calculated in three different ways*

(a) Calculated total scattering width, ***(b)*** Dependancy of surface reactance Z_{zz} on angular mode at 12 GHz

where k_{eff} is equal $k_{\text{eff}}^2 = k_0^2 \cdot (\varepsilon_r + 1)/2$. Note that the angle of incidence of the plane wave determines the spectral variable $k_z = k_0 \cos\theta$.

Fig. 4*a* shows that the approximations cause a frequency shift in the calculated scattering results. This frequency shift occurs because the rigorously obtained impedance tensor depends on the azimuthal mode. In contrast, the two approximations estimate the admittance tensor to be constant with respect to mode order m. This can be seen from the calculated surface reactances given in Fig. 4*b* at 12 GHz.

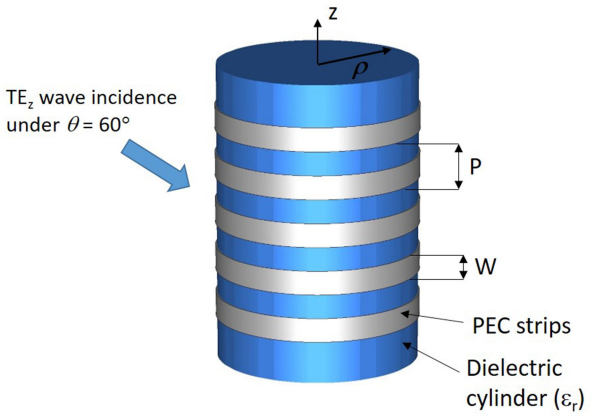

Fig. 5 *Dielectric cylinder with periodic circumferential PEC strips*

The situation is quite different for circumferential strips (Fig. 5). The periodicity of the strips is $P_z = 8$ mm ($0.27\lambda_0$ at 10 GHz), and all other parameters are kept the same as in the previous example. The incident wave was TE$_z$ polarised with incident angle $\theta = 60°$. Since we are considering the surface impedance in the spectral domain, we can modify the approximate planar surface impedance formulas (11) and (12) to include the propagation constant in the ϕ-direction $k_\phi = m/\rho$

$$Z_{zz}^{\text{approx}}(m) = -j\frac{\pi\eta_0}{P_z k_0(1+\varepsilon_r)}\left[\log\left(\csc\left(\frac{\pi W}{2P_z}\right)\right)\left(1-\frac{m^2}{\rho_{\text{strips}}^2 k_{\text{eff}}^2}\right)\right]^{-1} \quad (13)$$

$$Z_{\phi\phi}^{\text{approx}}(m) = j\frac{k_0\eta_0}{2\pi}P_z\log\left(\csc\left(\frac{\pi W}{2P_z}\right)\right)\left(1-\frac{m^2}{\rho_{\text{strips}}^2 k_{\text{eff}}^2}\right) \quad (14)$$

Note that the approximate formulas only have a dependence on the phase variation along the strips. Therefore, there is no dependency on incident angle θ in (13) and (14).

In this case, the surface impedance varies significantly with angular mode number (see Fig. 6*b*). Therefore, it is not possible to accurately approximate the surface impedance with the value obtained from the equivalent planar case. However, the approximate expressions (13) and (14) closely predict the azimuthal variation of surface impedance. Consequently, there is close agreement between the results in which the impedance tensor is determined using a cylindrical MoM code, the approximate expressions (13) and (14) in which the azimuthal variation is taken into account, and measurements (see Fig. 6*a*). One could also include the azimuthal propagation constant into the analysis of the equivalent planar structure. However, the equivalent incident angle will be different for each frequency and spectral variable m (i.e. the equivalent incident angle is equal to $\arcsin(m/(\rho_{\text{strips}}k_0))$), so it would be extremely time consuming to calculate the surface impedance using commercial EM solvers in this way.

3.2 Selection of optimal elements for cylindrical metasurfaces

To further verify the proposed method and indicate how different realisations of the metasurface effect the results, we will consider the mantle cloak example discussed in [16, 17]. The structure considered is a perfect electric conductor (PEC) cylinder of radius 10 mm, with a dielectric shell of outer radius 10.5 mm and permittivity $\varepsilon_r = 20$ shown in Fig. 7. The operating frequency is 3 GHz, therefore the radius of the PEC cylinder is $0.1\lambda_0$. The first step in designing a mantle cloak is to estimate the needed metasurface impedance. Initially, we assume that it has a constant value, i.e. that it does not change for different ϕ-modes. By performing a parametric sweep over sheet impedances and calculating the minimum total scattering width, it was determined

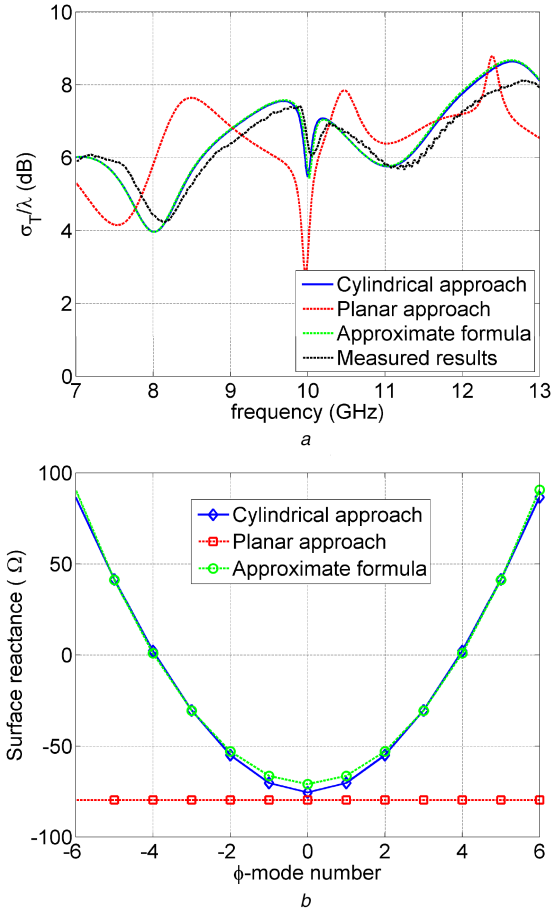

Fig. 6 *Comparison of calculated total scattering width of a dielectric cylinder loaded with periodic circumferential strips. The metasurface impedance is calculated in three different ways*
(a) Calculated total scattering width, ***(b)*** Dependency of surface reactance $Z_{\phi\phi}$ on angular mode at 12 GHz

that the optimal value for the metasurface reactance is −12.23 Ω. This is consistent with the results presented in [16]. We considered two realisations of the capacitive metascreen. The first realisation consists of square metallic patches shown in Fig. 7 (side width of $W = 10.6$ mm, and gap between the patches of $P–W = 0.39$ mm). The second realisation consists of Jerusalem crosses (Fig. 7) with side dimension $W_J = 9.382$ mm, line width $t_J = 0.625$ mm, T-section width $T_J = 3.127$ mm, and a gap between the crosses of $P_J–W_J = 1.61$ mm. In both cases, there are six elements along the ϕ-direction, i.e. period is $0.37\lambda_0$ at the central frequency. The values of surface impedance tensor are calculated using a MoM code for cylindrical periodic structures [20]. It should be noted that the dimensions of both structures were determined by finding those that resulted in minimum total scattering width at 3 GHz.

We have compared the total scattering width and the bandwidth properties of the cylindrical object with the two considered metasurface realisations in Fig. 8. The incidence wave is a TM_z polarised normally incident plane wave (i.e. $k_z = k_0 \cos\theta^{\text{inc}} = 0$). Fig. 8 also shows the result for a mantle cloak with constant metasurface reactance equal to −12.23 Ω, and the total scattering width of a PEC cylinder of radius 10.0 mm (i.e. of the hidden object) in order to establish the bandwidth of the considered cloaks. It can be seen that the patch metasurface is superior since it provides higher scattering reduction and larger bandwidth of operation. In addition, the patch metasurface outperforms the metasurface cloak with a constant sheet reactance. In order to explain why the patch metasurface is superior in comparison with the other structures, we have plotted the variation of the surface reactance with mode order m for all three considered cases. From Fig. 9, it is evident that all three cases have approximately the same reactance for the $m = 0$ mode (mode with no ϕ-variation). However, the surface impedance of the Jerusalem crosses and

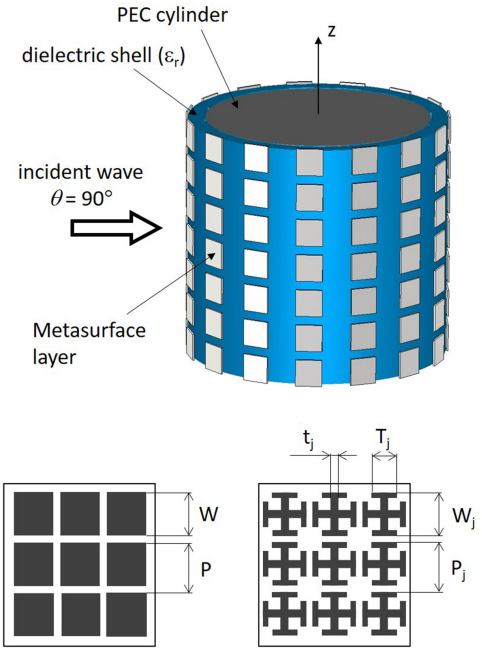

Fig. 7 *Mantle cloak realisation on a PEC cylinder with the dielectric shell. Cloak is a metasurface based on square PEC patches or PEC patches in the shape of Jerusalem crosses*

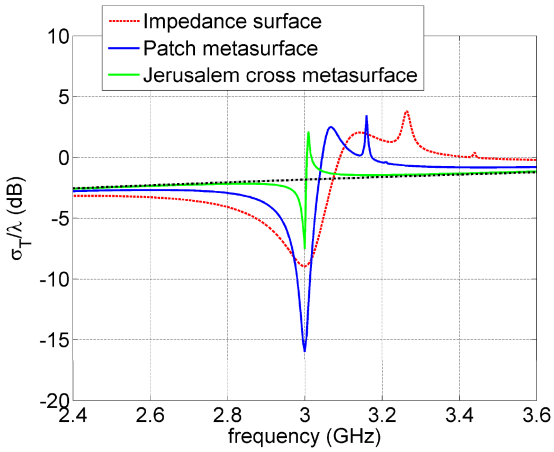

Fig. 8 *Comparison of calculated total scattering width of a dielectric cylinder loaded with metasurface. Total scattering width of a PEC cylinder of radius 10 mm is shown with black dotted line*

patches differs for the higher-order m modes. Specifically, the magnitude of the reactance is larger for patches than for Jerusalem crosses with increasing m. In order to appreciate the importance of tailoring the mode order variation of the surface reactance, we have calculated an optimum ϕ-variation for the surface reactance: the reactance that gives zero total scattering width for each ϕ-mode. This optimal impedance Z_{zz}^{opt} can be found by setting each spectral-domain component of the scattered field in (9) equal to zero, which results in a characteristic equation for each spectral component of the surface impedance

$$Z_{zz}^{\text{opt}}(m) = j\eta_0 \left(\frac{J'_m(k_0\rho_2)}{J_m(k_0\rho_2)} - \sqrt{\varepsilon_{r,1}} \frac{H_m^{(1)}(k_1\rho_1)H_m^{'(2)}(k_1\rho_2) - H_m^{(2)}(k_1\rho_1)H_m^{'(1)}(k_1\rho_2)}{H_m^{(1)}(k_1\rho_1)H_m^{(2)}(k_1\rho_2) - H_m^{(2)}(k_1\rho_1)H_m^{(1)}(k_1\rho_2)} \right)^{-1} \quad (15)$$

The optimum profile is also plotted in Fig. 9. It can be seen that the impedance profile of the patch metasurface closely resembles the optimal case. This example illustrates the importance of incorporating the spectral variation of a surface impedance into the design process.

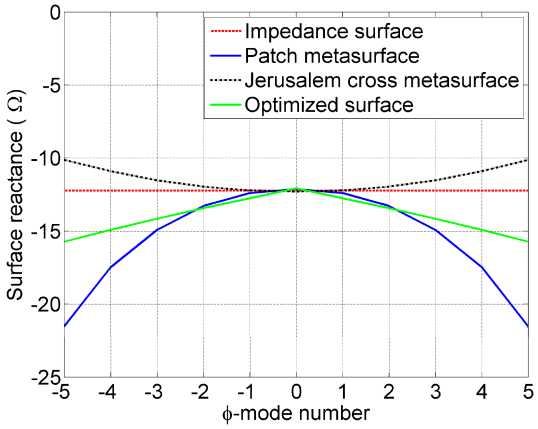

Fig. 9 *Dependency of the surface reactance of a dielectric cylinder loaded with metasurface on angular mode at 3 GHz*

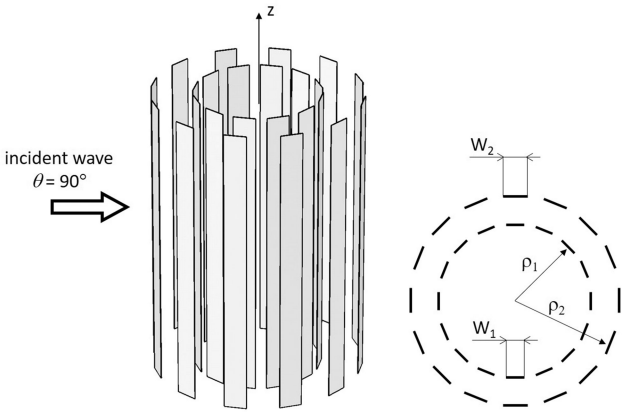

Fig. 10 *Two-layer periodic strip-grid cylindrical structure*

3.3 Analysis of a two-layer metasurface structure

As a final example, let us consider a two-layer cylindrical metasurface structure built from vertical strips. The intent of this example is to verify the proposed method on a multilayer design, and to investigate how close patterned sheets can be placed next to each other in order to still accurately model the structure using the ABCD transmission matrix approach. The approximation in the analysis method is that only the propagating (lowest-order) ϕ-modes are taken into account in the ABCD transmission matrix formulation. In other words, it is assumed that coupling between different metasurface layers occurs only through the considered propagating cylindrical mode with $\exp(jm\phi)$ variation, while higher-order Floquet modes (i.e. evanecent modes) are neglected. The higher-order Floquet modes are defined with azimuthal variation of the cylindrical mode $m_l = m + l \cdot N_\phi \; l \neq 0$, where N_ϕ is the number of periodic elements in ϕ-direction (strips in this case) and l is the Floquet-mode index. An equivalent assumption is commonly used in the planar case [24, 25].

In this example, we fixed the outer radius of the structure ($\rho_2 =$ 114.6 mm) and the number and width of the strips in each layer ($N_{\phi,1} = N_{\phi,2} = 24$, $W_1 = W_2 = 1.15$ mm; see Fig. 10). The working frequency was set to $f = 4.0$ GHz (i.e. strip period is $0.4\lambda_0$) and the excitation to a TM_z normally incident plane wave. The inner radius was selected to be 99.6, 103.3, and 107.1 mm. Therefore, the distance between layers was 0.2λ, 0.15λ, and 0.1λ, respectively. In Fig. 11, the calculated bistatic scattering width is plotted. There is good agreement between the two methods, the ABCD transmission matrix approach and the exact MoM code, even for close separation distances between the patterned sheets. The incoming plane wave is represented with 21 azimuthal modes, as suggested by the expression $N_\phi^{\max} \simeq (2\pi/\lambda_0)\rho_2$.

In order to estimate the distance at which higher-order evanescent modes should be taken into account, we calculated the EM field scattered by one strip layer and plotted the amplitude

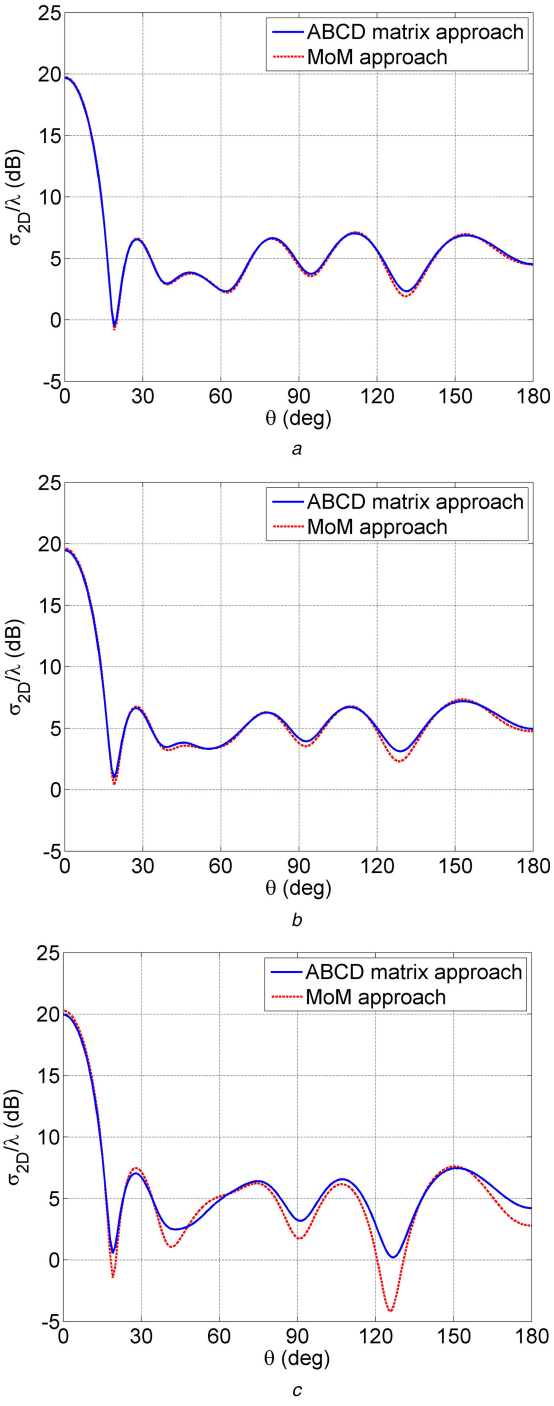

Fig. 11 *Scattered field from the two-layer periodic strip-grid structure; distance between two metasurface layers is*
(a) 0.2λ, ***(b)*** 0.15λ, ***(c)*** 0.1λ

decay of the evanescent modes as a function of distance from the periodic strip grid (see Fig. 12; the radial EM field variation is calculated using (2)). We considered the field variation in the outside region; the amplitude of each mode is calculated using the exact MoM program for cylindrical structures. The dominant $m = 0$ mode is considered, thus the higher-order Floquet modes are defined with $m = l \cdot N_\phi$, $l = 1, 2, 3$. A comparison of Figs. 11 and 12 reveals that the analysis can be improved with the inclusion of the ABCD matrices that account for higher-order (evanescent) modes for dielectric thicknesses where the higher-order modes have relative amplitudes larger than ~0.1 at the position of neighbouring metasurface layer. This can be done in the same way where both TE and TM modes are considered, as in the presented analysis method (see (6)–(9)).

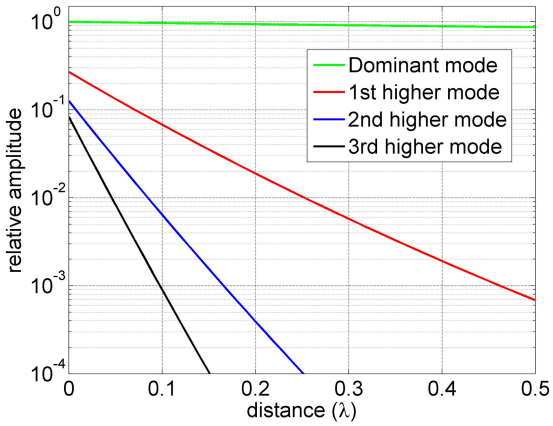

Fig. 12 *Decay of the amplitude of evanescent modes as a function of the distance from the periodic strip grid*

4 Conclusions

The paper discusses a spectral-domain surface impedance approach for analysing cylindrical cascaded metasurfaces. The reported approach extends the ABCD matrix formulation for the analysis of circuit networks or planar, stratified EM structures to canonical, curved geometries. The ABCD matrix formulation captures the interaction between sheets of the metasurface, while the individual sheets are modelled with surface impedances $\bar{\bar{Z}}$ in the spectral domain. The surface impedances can be determined either using a rigorous EM solver, such as the method of moments, or using approximate analytical expressions. These approximate expressions often assume that the surface impedance is constant with respect to spectral-domain angular variation of the incidence field. This leads to inaccuracies when $\bar{\bar{Z}}$ changes rapidly with respect to the spectral variable, i.e. if the considered metasurface has strong spatial dispersion. To account for this, the analytical formulas for the surface impedance of some planar metallic patterns have been modified to account for the considered angular Fourier harmonic. It has been shown, through calculations and comparison with measurements, that such canonical metasurfaces can be accurately modelled with the proposed approach. The approach can also aid in selecting the type of patterned sheet needed to obtain the desired variation in surface impedance $\bar{\bar{Z}}$ with modal number m.

5 Acknowledgments

This work was supported in part by the Air Force Office of Scientific Research, Air Force Material Command, USAF under award no. FA9550-15-1-0121, and by the project 'Passive and Active Metamaterial Structures for Guiding, Scattering and Radiation of Electromagnetic Energy', Unity through Knowledge Fund (UKF), Croatia.

6 References

[1] Munk, B.A.: '*Frequency selective surfaces: theory and design*' (John Wiley& Sons, Hoboken, 2005)

[2] Holloway, C.L., Kuester, E.F., Gordon, J., *et al.*: 'An overview of the theory and applications of metasurfaces: the twodimensional equivalents of metamaterials', *IEEE Antennas Propag. Mag.*, 2012, **54**, pp. 10–35

[3] Pfeiffer, C., Grbic, A.: 'Bianisotropic metasurfaces for optimal polarization control: analysis and synthesis', *Phys. Rev. Appl.*, 2014, **2**, pp. 1–11, Art. ID 044011

[4] Pfeiffer, C., Grbic, A.: 'Metamaterial Huygens' surfaces: tailoring wave fronts with reflectionless sheets', *Phys. Rev. Lett.*, 2013, **110**, pp. 1–5, Art. ID 197401

[5] Maci, S., Minatti, G., Casaletti, M., *et al.*: 'Metasurfing: addressing waves on impenetrable metasurfaces', *IEEE Antennas Wirel. Propag. Lett.*, 2011, **10**, pp. 1499–1502

[6] Kuester, E.F., Mohamed, M.A., Piket-May, M., *et al.*: 'Averaged transition conditions for electromagnetic fields at a metafilm', *IEEE Trans. Antennas Propag.*, 2003, **51**, pp. 2641–2651

[7] Zhao, Y., Belkin, M.A., Alù, A.: 'Twisted optical metamaterials for planarized ultrathin broadband circular polarizers', *Nat. Commun.*, 2012, **3**, pp. 870–876

[8] Pfeiffer, C., Grbic, A.: 'Cascaded metasurfaces for complete phase and polarization control', *Appl. Phys. Lett.*, 2013, **102**, pp. 1–4 Art. ID 231116

[9] Monticone, F., Estakhri, N.M., Alù, A.: 'Full control of nanoscale optical transmission with a composite metascreen', *Phys. Rev. Lett.*, 2013, **110**, pp. 1–5, Art. ID 203903

[10] Niemi, T., Karilainen, A., Tretyakov, S.: 'Synthesis of polarization transformers', *IEEE Trans. Antennas Propag.*, 2013, **61**, pp. 3102–3111

[11] Selvanayagam, M., Eleftheriades, G.V.: 'Polarization control using tensor huygens surfaces', *IEEE Trans. Antennas Propag.*, 2014, **62**, pp. 6155–6168

[12] Patel, A.M., Grbic, A.: 'Transformation electromagnetics devices based on printed-circuit tensor impedance surfaces', *IEEE Trans. Microw. Theory Tech.*, 2014, **62**, pp. 1102–1111

[13] Elek, F., Tierney, B.B., Grbic, A.: 'Synthesis of printed-circuit tensor impedance surfaces controlling phase and power flow', *IEEE Trans. Antennas Propag.*, 2015, **63**, pp. 3956–3962

[14] Raeker, B.O., Rudolph, S.M.: 'Arbitrary transformation of antenna radiation using a cylindrical impedance metasurface', *IEEE Antennas Wirel. Propag. Lett.*, 2016, **15**, pp. 1101–1104

[15] Raeker, B.O., Rudolph, S.M.: 'Verification of arbitrary radiation pattern control using a cylindrical impedance metasurface', *IEEE Antennas Wirel. Propag. Lett.*, 2017, **16**, pp. 995–998

[16] Chen, P.-Y., Alù, A.: 'Mantle cloaking using thin patterned metasurfaces', *Phys. Rev. B*, 2011, **84**, pp. 1–13, Art. ID 205110

[17] Padooru, Y.R., Yakovlev, A.B., Chen, P.-Y., *et al.*: 'Line-source excitation of realistic conformal metasurface cloaks', *J. Appl. Phys.*, 2012, **112**, pp. 1–11, Art. ID 104902

[18] Soric, J.C., Monti, A., Toscano, A., *et al.*: 'Dual-polarized reduction of dipole antenna blockage using mantle cloaks', *IEEE Trans. Antennas Propag.*, 2015, **63**, pp. 4827–4834

[19] Vellucci, S., Monti, A., Toscano, A., *et al.*: 'Scattering manipulation and camouflage of electrically small objects through metasurfaces', *Phys. Rev. Appl.*, 2017, **7**, pp. 1–12, Art. ID 034032

[20] Sipus, Z., Raffaelli, S., Kildal, P.-S.: 'Periodic strips on planar and circular cylindrical substrates: exact and asymptotic analysis', *Microw. Opt. Technol. Lett.*, 1998, **7**, pp. 173–178

[21] Luukkonen, O., Simovski, C.R., Grant, G., *et al.*: 'Simple and accurate analytical model of planar grids and high-impedance surfaces comprising metal strips or patches', *IEEE Trans. Antennas Propag.*, 2008, **56**, pp. 1624–1632

[22] Simovski, C.R., De Maagt, P., Melchakova, I.V.: 'High-impedance surfaces having stable resonance with respect to polarization and incidence angle', *IEEE Trans. Antennas Propag.*, 2005, **53**, pp. 908–914

[23] Pozar, D.M.: '*Microwave engineering*' (John Wiley & Sons, Hoboken, 2011)

[24] Vardaxoglou, J.C.: '*Frequency selective surfaces*' (Research Studies Press Ltd., Taunton, England, 1997)

[25] Shuley, N.V.: 'Higher-order mode interaction in planar periodic structures', *Proc. IEE-H*, 1984, **131**, pp. 129–132